

MAGNETIC TOPOLOGIES: WHERE WILL RECONNECTION OCCUR ?

Pascal Démoulin

Observatoire de Paris, section de Meudon, LESIA, UMR 8109 (CNRS), F-92195 Meudon Cedex, France

ABSTRACT

The energy needed to power flares is thought to come from the coronal magnetic field. However, such energy release is efficient only at very small scales. Magnetic configurations with a complex topology, i.e. with separatrices, are the most obvious configurations where current layers can spontaneously form. 3-D magnetic configurations have a variety of magnetic topologies not suspected before. If the photospheric field is described by an ensemble of magnetic charges, separated by flux-free regions, a complete topological description of the associated potential field is provided by the skeleton formed by the null points, spines, fans and separators. In order to better match the observed photospheric magnetograms, the magnetic charges can be set below the photosphere; then an extra topological element can appear, so-called bald patches with associated separatrices. In several flaring configurations the computed separatrices allows to understand the localization of the flare ribbons in the framework of magnetic reconnection. However, this view is too restrictive taking into account the variety of observed solar flaring configurations. Indeed “quasi-separatrix layers” (QSLs), which are regions where there is a drastic change in field-line linkage, generalize the definition of separatrices for magnetic fields extending in the full volume (photosphere and corona). The concept of “hyperbolic flux tube” (HFT) also generalizes the concept of separator. These studies indeed teach us that coronal magnetic reconnection occurs in a broader variety of magnetic configurations than traditionally thought, and this variety is reviewed.

Key words: Magnetic reconnection; Magnetic topology; Magnetic fields; flares .

1. MAGNETIC ENERGY RELEASE

The transformation of magnetic energy takes various forms in the solar atmosphere ranging from coronal mass ejections and flares down to the very small events implied in quasi-continuous coronal heating. Magnetic reconnection is thought to be at the heart of the energy conversion

processes. Since the magnetic Reynolds number is typically of the order of 10^{10} , when global scales are considered, magnetic energy dissipation can only occur efficiently when small spatial scales are created in the magnetic field. One way is the development of MHD turbulence. Another way is the creation of thin current layers during the evolution of the configuration. Both ways are indeed related, but below I focus only on the second one, more precisely on the topology of the coronal magnetic field as a basic concept to understand where energy could be released in a highly conductive plasma.

Magnetic configurations with a complex topology, i.e. with separatrices, are the most obvious configurations where current layers can form (Section 2). These separatrices are associated to magnetic **null points** in the corona (where the magnetic field vanishes) or to field lines tangent to its lower boundary (the photosphere, in practice), at locations called **bald patches**. These concepts let us understand part of the energy-release events (such as flares), but not all of them. This has motivated an extensive research on magnetic topology. The earlier studies are summarized in Section 3. Then, further investigations are divided in two main branches: the topology of magnetic fields formed by a series of separated flux tubes at the photospheric level (Section 4) and the extension of the concept of separatrices to QSLs for general magnetic fields anchored to a boundary (Section 5). Finally, these approaches are critically compared in Section 6. Other recent reviews on the subject will soon be published (Démoulin 2005; Longcope 2005; Titov 2005).

2. MAGNETIC SEPARATRICES

2.1. From 2D to 3D configurations

Separatrices are magnetic surfaces where the magnetic field line linkage is discontinuous. The simplest example is a 2-D magnetic configuration with an X-point (where the magnetic field vanishes). Two separatrices cross at the X-point, and they define four separated regions, **connectivity domains**, where the magnetic connectivity change continuously for one field line to its neighbor. 2D bound-

ary flows invariably lead to the transformation of the X-point into a current sheet when equilibrium configurations are considered (e.g. Sweet 1958; Low 1987).

Next, let consider 3D configurations invariant in one direction (so called 2.5-D configurations). They are similar to the above 2-D magnetic configurations, except that a third field component is present in the invariant direction. Current sheets form along the whole separatrices when shearing flows are present around the photospheric footprint of separatrices (e.g. Zwingmann et al. 1985). This occurs in two distinct cases as follows. Firstly, when there is an X-point in the direction of poloidal field (orthogonal to the invariance), as in the 2-D case (Low & Wolfson 1988; Finn & Lau 1991; Vekstein & Priest 1992). Secondly, when there are field lines tangent to the photospheric boundary (then, they are curved upward, Wolfson 1989; Low 1992; Vekstein & Priest 1992). The general definition of these locations is given by Titov et al. (1993). They called them **bald patches** (BPs) with the visual reference to a haircut (field lines being associated to hairs). The two cases above have a generalization in 3-D magnetic configurations: separatrices are formed by field lines which thread either null points or bald patches.

2.2. Null points and bald patches

The vicinity of a null point is usually described by the second (linear) term in the local Taylor expansion of the magnetic field. The diagonalisation of the field's Jacobian matrix provides three orthogonal eigenvectors (Molodenskii & Syrovatskii 1977). The divergence-free condition imposes that the sum of the three eigenvalues vanishes ($\lambda_1 + \lambda_2 + \lambda_3 = 0$), and for magnetic fields in equilibrium with a plasma ($\vec{j} \times \vec{B} = \vec{\nabla}P$) the eigenvalues are real (Lau & Finn 1990). Then two eigenvalues, say λ_1, λ_2 , have the same sign, opposite to the one of the third eigenvalue λ_3 . The two **spines** of the null are defined by the two field lines which start from an infinitesimal distance of the null in directions parallel and anti-parallel to the eigenvector associated to λ_3 (Fig. 1). The **fan** surface is defined by all the field lines starting at an infinitesimal distance of the null in the plane defined by the two eigenvectors associated to λ_1 and λ_2 . Two types of nulls exist depending on the sign of the fan eigenvalues; their sign is used to define the sign of the null (another convention is to call them A & B types: A is for a negative, and B is for a positive null). The spines and fan are defined by the local properties of the null, but they have large scale implications for the topology of the magnetic field since field lines on both sides of a fan connect, in general, far distant magnetic regions: a discontinuity in the magnetic connectivity is present across a fan, so a fan generically defines a separatrix (an unusual exception exists: when the two spines of the null connect the same charge). Finally, the intersection of the fans of two nulls of opposite signs define a magnetic **separator**.

At the opposite of the genuine separatrix defined by mag-

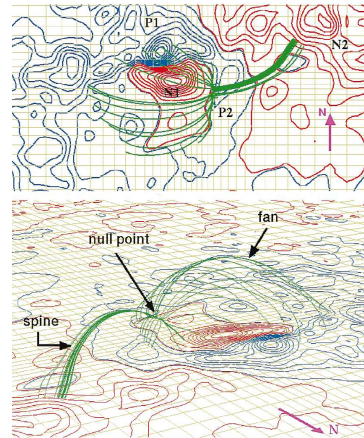


Figure 1. Example of a magnetic null point found in a flaring configuration in the vicinity of a δ spot. Isocontours of the magnetogram are shown with blue/red lines for positive/negative values. Field lines (green lines) passing very close to the null point are grouped along the spines and spread all along the fan. Observational evidences of reconnection at the null are interpreted in the "magnetic breakout" process which triggers the associated eruptive flare (from Aulanier et al. 2000).

netic nulls, the separatrix defined by a bald patch requires the existence of a boundary. In the solar atmosphere the sharp transition of regime (e.g. from low to high beta values) from the corona to the photosphere is used to introduce such lower boundary. In a gravitationally stratified photosphere, the numerical simulations of Karpen et al. (1991) showed that, instead of current sheets, current layers of finite thickness are formed. However, Billinghurst et al. (1993) showed, that if the field strength decreases sufficiently rapidly towards the place of field line contact with the photosphere, the current layers in the corona could still be much thinner than the photospheric gravitational scale height. Then, Titov et al. (1993) explored part of the space of parameter for 3D configurations formed by four magnetic charges with one main and one small bipole. They showed that a bald patch exists at the center of their analyzed configuration for a wide range of parameters. Bungey et al. (1996) studied the splitting, or bifurcation, of such a bald patch when the small bipole has an increasing strength. This bifurcation gives birth to a separator at the intersection of the two separatrices associated with each bifurcated bald patch. That is presently the only known example of a separator which is not caused by the presence of two magnetic null points. Such kind of separator was also found in other kind of configurations, for example in a strongly twisted configuration modelling an active region (Fig. 2).

A particularly important location for magnetic reconnection (in a classical view) is the separator. The intersecting separatrices define four domains of connectivity. During the evolution of the configuration, two set of field lines from opposite domains are brought toward each other. A current sheet is usually first formed; then, the field lines are reconnected to form new field lines in the other two

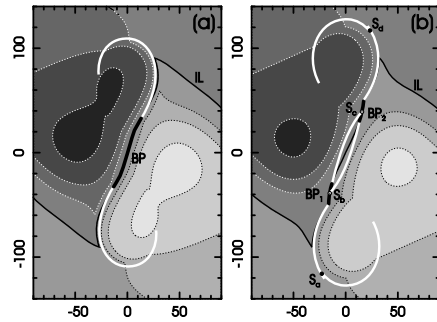


Figure 2. Bald patches (thick black lines) and the “photospheric” footprint of their separatrices (thick white lines) in a model of a twisted flux tube in equilibrium in an active region-like field. In (a) only one bald patch is present, while it has bifurcated in two in (b), giving birth to a separator which photospheric footprints are S_a, S_b, S_c, S_d . The grey levels and the isocontours represent the theoretical “photospheric” magnetogram (from Titov & Démoulin 1999).

domains (Greene 1988; Lau & Finn 1990). Finally, both for separatrices associated to nulls or to bald patches, current sheets are thought to form all along the separatrices when arbitrary foot-point motions are imposed at the photosphere around the separatrices (e.g. Aly 1990; Lau 1993); so potentially, all the separatrices are locations where magnetic reconnection can easily occur.

2.3. Observational tests

Testing the above theory for the spatial localization of the energy-release sites needs the computation of the coronal magnetic field from observed photospheric magnetograms. It also needs the clearest indirect evidences of energy release (e.g. flare ribbons and loops).

Some of the studied flaring active regions (ARs) have indeed a magnetic null point in the extrapolated coronal fields: e.g. when an almost oppositely oriented bipole emerged between the two main polarities of an AR (e.g. Mandrini et al. 1993; Gaizauskas et al. 1998), but also in some other configurations (Aulanier et al. 2000; Fletcher et al. 2001b). The magnetic null position is weakly sensitive to perturbations of the magnetic configuration (e.g. modifying the photospheric magnetogram, or the coronal currents) when the absolute value of the three eigenvalues are comparable. In particular, this stable case is present when the null is above a photospheric magnetic polarity surrounded by significant fields of opposite polarity (Fig. 1). At the opposite, when one eigenvalue magnitude is much lower than the others, the spatial position of the null is structurally unstable (Gorbachev et al. 1988). Finally, in the analyzed flares, the found nulls can be at any location along the separator (close to its top, or close to the photosphere), without having a spatial relationship with the brightest part of the kernels (Démoulin et al. 1994a).

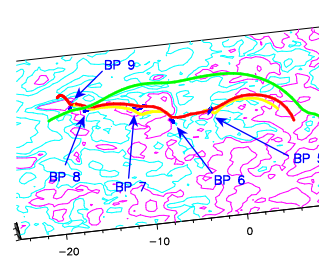
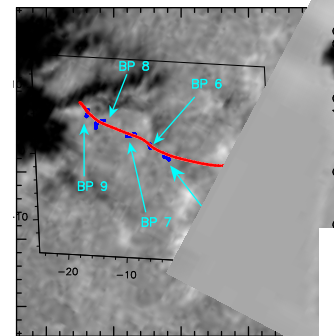


Figure 3. Examples of bald patches (dark blue) found in an emerging region in relation with Ellerman bombs (a signature of magnetic energy release). The majority of the Ellerman bombs are found at the locations of the bald patches or at the end of their related separatrices. Three examples of the associated field lines are drawn with thick lines (green, red, yellow). The magnetogram is shown as an image (resp. with pink/blue lines for positive/negative isocontours) in the top (resp. bottom) panel (from Pariat et al. 2004).

Bald-patch separatrices have been related to the spatial location of various brightenings. The theory predicts that large scale events can occur, in association with X-ray sigmoids (Fig. 2), but so far, bald patches were found only in minor events such as a small flare (Aulanier et al. 1998), in transition region brightenings (Fletcher et al. 2001a), in surge ejections (Mandrini et al. 2002), and in interconnecting arcs between two ARs (Delannée & Aulanier 1999). Pariat et al. (2004) found that reconnection at bald-patch separatrices is a key process during the emergence of magnetic flux through the photosphere (Fig. 3). When a buoyant flux tube reaches the top of the convective zone, it cannot continue coherently its ascension through the photosphere because the external atmosphere is so weakly dense compared to its own plasma density. An almost horizontal field then accumulates below the photosphere until the Parker instability sets in and creates wavy-like field lines. The curved-down parts of the flux tube can continue their emergence through the photosphere since the dense plasma can flow along the legs, but the curved up parts cannot since dense plasma accumulates there. It is only with magnetic reconnection at the bald-patch separatrices that the flux tubes can finally emerge. Pariat et al. (2004) provided observational evidences of this progressive transformation of the wavy-like photospheric flux tubes to the arch-like coronal flux tubes.

In conclusion, there are many observed cases where the separatrices of coronal nulls or bald patches let us understand the spatial localization of the energy release. However, in several ARs no such coronal null point, or bald patch, can be found and linked to the evidences of energy release. Of course, it is possible that the magnetic modelling of the coronal field is not close enough to the real one (with the exception that the location of bald patches themselves can be deduced directly from vector magnetograms when the 180° ambiguity is resolved). In fact, for several analyzed cases, it is difficult to imagine how a coronal null, or a bald patch, can exist in any reasonable magnetic configuration associated to the observed photospheric field and that its associated separatrices can explain the observed ribbons and flare loops (Démoulin et al. 1994a).

3. EARLIER STUDIES

At the time of the initial studies of the topology of flaring configurations, the description of the magnetic topology, as summarized in the previous section, was only partially known. These studies rather took into account the fact that the observed photospheric magnetic field is dominantly concentrated in flux tubes. This was modeled using discrete magnetic sources (charges or dipoles). The magnetic null points present between these sources are implicitly at the origin of a complex topology.

Sweet (1958) proposed a model formed by four magnetic sources, two being positive and two being negative. These sources are linked by four kinds of field lines, defining four **connectivity domains**. Then, Baum & Bratenahl (1980) calculated numerically the location of separatrices for a potential magnetic field generated by four magnetic charges. They showed that the magnetic topology cannot be deduced neither from the magnetogram nor from a set of randomly selected field lines. Hénoux & Somov (1987) proposed that reconnection along the separator interrupts currents flowing along lines of force releasing the energy stored in these currents. Then, Gorbachev & Somov (1988, 1989) developed the theory and applied it to an observed flare, showing that field lines passing close to the separator connect approximately to the chromospheric flare ribbons.

The next logical step was to introduce many sources (charges or dipoles, Mandrini et al. 1991, 1993) and to determine their position and intensity by a least-square fitting of the computed magnetic field to the observed one (Démoulin et al. 1994b). In these cases, many separatrices are present and the sources should be gathered in groups; that is to say, all the sources used to describe the observed complex shape of one field concentration, like a sunspot, belong to the same group. The connectivity of a field line is then defined by the groups to which the sources, found at both of its ends, belong. A region, where the same two groups are found, define a connectivity domain. The domains are separated by separatrices. This defines the **source model**.

Detailed analyses of various flares using the source model have shown that $H\alpha$ and UV flare brightenings are located along the intersection of separatrices with the chromosphere; moreover, they are connected by field lines which are expected to form through reconnection in the given configuration (Mandrini et al. 1991, 1993, 1995; Démoulin et al. 1993, 1994b; van Driel-Gesztelyi et al. 1994; Bagalá et al. 1995). These results are valid for a variety of observed magnetic configurations, from quadrupolar ARs to bipolar ones with an S-shaped inversion line. Moreover, when available from transverse field measurements, the photospheric electric currents have been found at the border of the separatrices.

4. MAGNETIC CHARGE TOPOLOGY (MCT)

4.1. Definitions and assumptions

The **MCT model** assumes that the photospheric field can be partitioned into many isolated unipolar regions (which are the trace of the sub-photospheric flux tubes Longcope & Klapper 2002). Each sub-volume where coronal field lines connect the same two unipolar regions define a **connectivity domain** and the boundaries between the domains define the **separatrices** (as in previous models with sub-photospheric sources).

Since the definition of the unipolar regions, and in practice the charges, are at the heart of the magnetic topology defined by the MCT model, a powerful method is needed to define them in a magnetogram. This is relatively easy in the quiet Sun since most of the magnetic flux is localized in thin flux tubes with strong fields (e.g. Close et al. 2003). For active regions (ARs), in particular their plages, the partitioning is more difficult due to the presence of many flux tubes partially stack together. Taking a minimum threshold value on the normal field component $|B_n|$ is not sufficient to separate all the regions, e.g. when there is a relative low valley in between two maxima of $|B_n|$, and a further manual, so subjective, step is needed to define the unipolar regions (Longcope & Silva 1998). An automatic algorithm was derived by Schrijver et al. (1997). The labels of regions are set by working in descending order of $|B_n|$. Each step considers a magnetogram pixel. If the eight neighbors have not yet a label, the central pixel is a local maximum and a new label is associated to it, while if some neighbors have already a label, the one with the greatest $|B_n|$ value is used to define the label of the central pixel. This method defines a unique label for every pixel. All pixels sharing a common label define a single unipolar region. Since this define, in general, a large number of regions for an AR, the smaller regions are grouped with others using criteria on the magnetic flux and field strength.

A further step is needed to build an MCT model since it requires isolated unipolar regions (with $B_n = 0$ all around them). This condition is achieved by replacing the unipolar regions by magnetic charges with the same

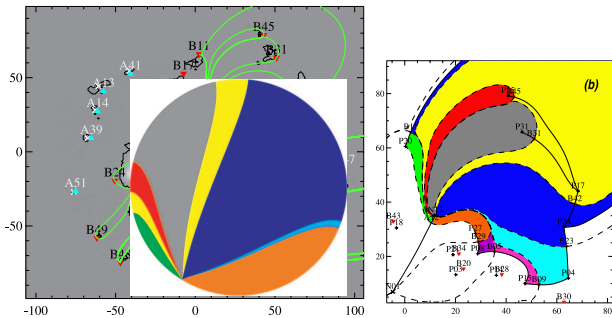


Figure 4. Magnetic topology of AR 8210 within an MCT model. The left panel shows the magnetogram (grey levels) and the defined partitions of flux (marked with black lines). Each partition is replaced by a magnetic charge of equivalent coronal flux, located at the flux center of the region. The photospheric magnetic nulls, in between the charges, were computed with a potential field (blue for A-type, red for B-type). Separators (green lines) are field lines joining two nulls. More than one separator can connect to a single null. The right panel shows a part (top left) of the left panel with the connectivity domains (colors), the spines (solid lines) and fan traces (dashed lines) (from Barnes et al. 2005).

coronal flux. They are all positioned at the magnetogram level (or charge plane) and at the flux weighted centre of the regions (Fig. 4). This corresponds to a multipolar expansion, limited to the first two terms (monopolar and dipolar), for the potential field created by each region. This expansion is precise only at a distance much larger than the size of the regions. In particular, the photospheric magnetogram is replaced by $B_n = 0$ everywhere except at the charge locations, and the coronal field, at low height, is much more concentrated than the corresponding direct potential-field extrapolation of the magnetogram. These transformations are justified by the structural stability of magnetic topology.

The MCT model retains the coronal nulls, but not the bald patches described in Section 2. However, the condition $B_n = 0$, at most places of the charge plane, introduces many new magnetic nulls. Their locations are defined by the conditions that the two field components, tangential to the charge plane, vanish. Then, finding these nulls is easier than finding the coronal nulls (search in a 2D domain rather than in a 3D domain). These nulls have also a special property: one of the eigenvector is normal to the charge plane. Either this eigenvector defines both spines, either it is part of the fan. The nulls are called **upright** and **prone nulls**, respectively. The upright nulls do not separate coronal domains. They are also much less numerous than the prone nulls; for example in a configuration formed by randomly distributed charges, the number of upright nulls per charge is maximum when all charges have the same polarity; this maximum is, in average, about 1 upright null for 11 prone nulls (Beveridge et al. 2002). Then, for the topological analysis, the prone nulls are the most relevant. The surrounding field lines form in the charge plane an hyperbolic structure similar

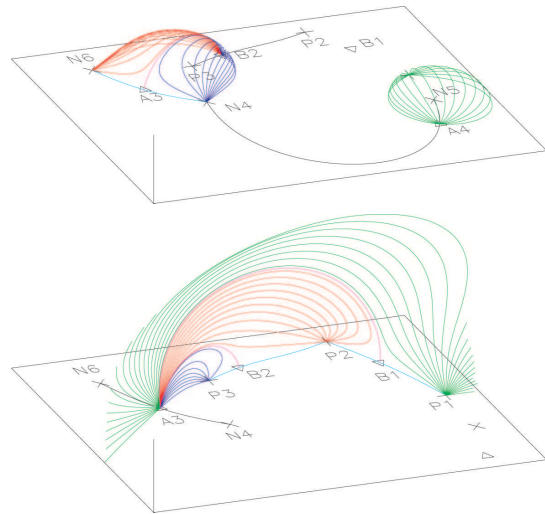


Figure 5. Examples of fan surfaces. The magnetic charges (+: positive, -: negative) and the null points (A3,A4,B1,B2) are all in the charge plane while the field lines (in color) extend above. The black and light-blue thin lines are the spines of the nulls. In the top panel the fan of null B2 is broken into two sectors by a separator going from B2 to A3, while the fan from null A4 is unbroken (all its field lines go to the charge P1). In the bottom panel, the fan from null A3 is broken twice by the separators going to nulls B2 and B1 (from Longcope & Klapper 2002).

to the one present around 2D null points. The prone nulls are frequent, typically their number is close to the number of charges, and it is frequent to have a prone null in between two charges.

4.2. Magnetic topology

The coronal nulls and the prone nulls are the base of the magnetic topology defined by an MCT model. Since coronal nulls are so rare, the analysis is frequently limited to the prone nulls. The fan of each prone null define generically a separatrix separating two connectivity domains. An example is shown on the top panel of Fig. 5, the fan of null A4 is unbroken and it fully encloses the domain linked to charge N5. When the fans of two nulls (of opposite sign) intersect, this defines a separator; four connectivity domains are in contact at a separator. For example, in the top panel of Fig. 5, the fan of null B2 (outlined with field lines) intersects the fan of null A3 (not shown) and a separator joins A3 to B2. This last case is equivalent to the configuration analyzed in earlier studies (Section 3).

The magnetic topology can become rapidly complex as the number of nulls increases, in particular because several separators can be rooted in a single null (Longcope & Klapper 2002). The bottom panel of Fig. 5 shows a case where the fan of null A3 hosts two separators (ending at

nulls B1 and B2). The presence of multi-separators ending in a null is also found in models of ARs (e.g. Fig. 4).

The complex topology of any MCT field is summarized by the so-called **skeleton** formed by all the null points, their spines, fans and separators (right panel of Fig. 4). Longcope & Klapper (2002) described a systematic method to analyse the skeleton. Because the complexity and variety of possible skeletons increase rapidly with the number of charges, the classification of all the possible skeletons has only been done, so far, for the cases with 3 and 4 unbalanced charges (Priest et al. 1997; Brown & Priest 1999, 2001; Beveridge et al. 2002; Pontin et al. 2003).

As the charges are modified (locations or intensities) the magnetic topology can be transformed when a local or global bifurcation occurs. **Local bifurcations** create or destroy null points without changing the number of domains present (but only their shapes). The generic case is the creation (or destruction) of two nulls of opposite signs (Brown & Priest 2001). The two nulls are created with intersecting fans, so they are linked by a separator. In the charge plane, the assumed symmetry of the MCT model forbids this generic bifurcation (the field below the plane is the reflective symmetry from above). Rather a null is transformed (or the reverse) to three nulls: one stays in the plane, one drifts above and the third one is the symmetric image below. **Global bifurcations** have a stronger effect on the topology since they create or destroy domains. The most important are the global separator bifurcation and the spine-fan bifurcation (Brown & Priest 1999). With the first one, the fans of two nulls of opposite sign encounter creating a pair of separators (Gorbachev et al. 1988). At least one new domain is created. With a spine-fan bifurcation, the spine of one null encounters the fan of a like-sign null. There is an exchange of connectivities between two charges and usually a complex effect on the domains.

4.3. Observational tests

Any portion of the quiet Sun, say 100 Mm wide, has a great topological complexity. Schrijver & Title (2002) made a statistical analysis with a random distribution having a few hundred charges with global flux balance. They found, in average, that a charge is connected to 8 opposite charges. The majority of the flux is in short connections, however there are also some very long connections to distant charges. Then, analyzing the topology of magnetograms with the same method, they found only evidences of the shortest connections, as predicted by the potential field model, in the EUV observations. Close et al. (2003) analyzed other quiet Sun magnetograms and found, in average, slightly less connections per charge: between 4 and 7. Still the magnetic topology of the quiet Sun is very complex, with numerous connectivity domains and separators, and so with many locations where magnetic reconnection can be forced by the perpetual motions of photospheric flux tubes.

The topological complexity can also be present in unipolar regions separated in many flux tubes. A model with a random distribution of charges gives a mean of 20 connections to the charges in the opposite unipolar region (Beveridge et al. 2003). It gives a picture of energy release in each coronal loop fragmented in many locations, confirming the previous results of Démoulin & Priest (1997) obtained with a QSL analysis (Section 5).

A clear case where magnetic reconnection should have occurred is shown by the coronal loops linking two ARs, which have emerged at different times. In an example of an AR emerging nearby an older one, Longcope et al. (2005) found that most magnetic reconnection occurred in a 3-6 hours interval with an onset delayed by approximately 24 hours following the onset of flux emergence. An MCT model let us to understand the spatial location of the interconnecting loops: they are found in one domain connecting the two ARs. Only about 25% of the flux in this domain could be found in the observed interconnecting loops, suggesting that most of the reconnected loops stay at temperatures larger than ≈ 2 MK. Finally, a pair of flux tubes is created in any reconnecting event, but this other set of reconnected loops was not observed, probably due to their too large and too faint nature.

Another clear case, showing the consequences of magnetic reconnection, is in a flare, especially when it is due to the emergence of new flux. Longcope & Silva (1998) interpreted the soft X-rays loops of a flare using an MCT model of the magnetogram. They associated the three observed loops to three separators. Two separators are rooted in the same prone null. The model predicts a high probability of simultaneous flaring on these two separators, and indeed sympathetic flaring of the corresponding loops was observed.

One advantage of the MCT model is that the charge strength measures precisely the amount of magnetic flux entering in the corona (while for submerged charges, part of the flux never crosses the photosphere, and the amount of lost flux depends on the positions of all charges). Then, by modelling the magnetic evolution of a region, it is possible to follow the flux evolution of each connectivity domain, and then the amount of reconnected flux at each separator if the field stays potential (Longcope et al. 2005). Another development is to model the build up of magnetic energy assuming that, during the phase preceding a flare, no reconnection occurs at the separators, while reconnection is so efficient elsewhere that the field stays potential. Then, currents are only in current sheets at the separators. This minimizes the magnetic energy under the constraints of fixed magnetic flux in each domain (Longcope 2001). It is worth to note that, this hypothesis of energy storage in current sheets is a long standing paradigm in solar physics (see e.g. Somov 1992, and references therein), while it is not at all clear that the strong current density, present in current sheets, can be dissipated at a much lower rate than the distributed coronal currents. According to the above flux-constrain model, a current layer develops along the separator until some threshold is reached, which produces a flare. An MCT

model of a flaring configuration then permits to estimate the threshold parameter (Longcope & Silva 1998).

5. QUASI-SEPARATRIX LAYERS (QSLs)

In the previous Section the concept of separatrices is remaining because, at the photospheric level, the magnetic field is supposed to be all confined in separated flux tubes; then all the magnetogram is replaced by the magnetic field created by few tens of magnetic charges. At the opposite, in this section, the observed magnetogram is fully kept. A consequence is that there are not necessarily separatrices to interpret the observed brightenings, but a generalization of the concept of separatrices does provide an interpretation in the framework of 3-D magnetic reconnection. There is also a clear theoretical need to generalize the concept of separatrices in 3-D configurations as illustrated in the following basic example. Let's consider a quadrupolar magnetic configuration invariant in one (y) direction. The intersecting separatrices define four domains of connectivity. However, when the magnetic configuration has a finite extension in the y direction, in many cases there are no longer separatrices. The structural instability of separatrices, when going from 2.5-D to 3-D, was first pointed out by Schindler et al. (1988) in the case of twisted magnetic configurations. However, this structural instability is no longer present when the notion of separatrices is generalized to that of QSLs (Démoulin et al. 1996b). This indeed complements the theory of Schindler et al. by localizing the regions where enhanced resistivity, and so reconnection can occur.

5.1. Definition of QSLs

Magnetic reconnection is most generally defined as the process that cuts and re-assembles magnetic field lines. The photospheric evolution imposes slowly evolving boundary conditions to the coronal magnetic field. So let us consider the field line mapping from one photospheric polarity to the opposite one: $\vec{r}_+(x_+, y_+) \mapsto \vec{r}_-(x_-, y_-)$ and the reversed one $\vec{r}_-(x_-, y_-) \mapsto \vec{r}_+(x_+, y_+)$ which can be represented by some vector functions ($X_-(x_+, y_+), Y_-(x_+, y_+)$) and ($X_+(x_-, y_-), Y_+(x_-, y_-)$), respectively. Let us define the norm $N_{\pm} \equiv N(x_{\pm}, y_{\pm})$ of the respective Jacobian matrix of both mappings. A QSL was first defined by the condition $N_{\pm} \gg 1$ in both photospheric polarities (Démoulin et al. 1996a; Priest & Démoulin 1995). The QSLs extend in the volume following the magnetic field lines anchored in the regions $N_{\pm} \gg 1$.

Let us consider a field line linking the photospheric locations (x_+, y_+) to (x_-, y_-) having a normal field component B_{n+} and B_{n-} , respectively. A difficulty with the definition of N_{\pm} is that $N_+ \neq N_-$ if $B_{n+} \neq B_{n-}$, so that a QSL does not fulfill a unique condition. A better way is to define a function which is independent of the

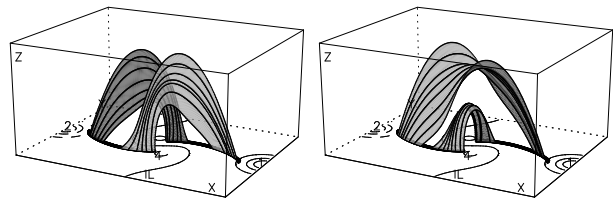


Figure 6. Perspective view of a simple configuration formed by four “photospheric” field concentrations (continuous and dashed lines are isocontours of the vertical field component). The footprints of the QSLs on the lower boundary are shown with thick black lines (isocontours of the norm N). Along the borders of the QSLs four sets of field lines are shown (adapted from Démoulin et al. 1996a).

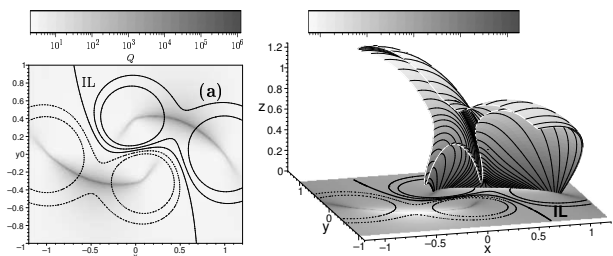


Figure 7. QSLs of a potential magnetic configuration. **Left:** the “photospheric” distribution of Q (Eq. 1) superimposed with the magnetogram (isocontours). **Right:** the QSLs are drawn for the magnetic surface $Q = 100$. This surface is cut mid-way to better show the X shape of the QSLs. The important thickness of the QSLs is only due to the low Q value selected for viewing purposes. QSLs in this configuration in fact define a very flat volume (from Titov et al. 2002).

mapping direction such as the squashing degree Q :

$$Q_+ = \frac{N_+^2}{|B_{n+}/B_{n-}^*|} \quad \equiv \quad Q_-^* = \frac{N_-^{*2}}{|B_{n-}^*/B_{n+}|}, \quad (1)$$

where the asterisk in the functions indicates that their arguments x_- and y_- are substituted on $X_-(x_+, y_+)$ and $Y_-(x_+, y_+)$, respectively. Then, a QSL is defined by $Q_+ = Q_- = Q \gg 2$ (Titov et al. 2002). A tiny circular region in one polarity is mapped to a very elongated elliptical region in the other polarity inside a QSL. Then Q simply measures the aspect ratio of this ellipse; in other words, how much the initial region is squashed by the field-line mapping. This new definition is linked to the previous one by the product of N values found at both footpoints of field lines ($Q = N_+ N_-^*$).

5.2. Main properties of QSLs

The main QSL properties, as derived from the analysis of several flares and theoretical configurations, are summarized below.

QSLs include, as a limit case when $Q \rightarrow \infty$, the concept of separatrices (associated both to magnetic null points and bald patches). With separatrices the mapping is so drastic that it is discontinuous.

From a mathematical point of view, a QSL of finite width is not a topological object like a separatrix, since this QSL can be removed by suitable continuous deformations of the magnetic field. But in the corona, I conjecture that the same physics is occurring at a separatrix and at QSL which is thin enough, as follows. In the framework of ideal MHD, almost any evolution of the magnetic configuration creates an infinitely thin current sheet along a separatrix and a current layer of finite width along a QSL. However, in the corona, local physical processes, like resistivity or kinetic processes, broaden any current region to a finite width. Then, for the physical evolution of coronal fields, there is no basic difference between a separatrix and a QSL provided that the QSL is thinner than the sizes given by the “microscopic” physics.

The basic magnetic configuration having QSLs is formed by two interacting magnetic bipoles (model by four sub-photospheric magnetic charges). When the bipoles are nearly anti-parallel, the configuration has intersecting separatrices (Hénoux & Somov 1987; Lau 1993). When the bipoles are slightly less anti-parallel, only QSLs of finite thickness remain (Démoulin et al. 1996a). QSLs persist, while becoming thicker, as the two bipoles are becoming more parallel. In all cases, the magnetic field line linkage has four basic sets of magnetic connectivities (Fig. 6), just as in 2-D quadrupolar magnetic configurations.

The spatial properties of QSLs are best illustrated in the simple bipolar configuration of Fig. 7. The intersection of the QSLs with the boundary is formed only by two extended thin stripes, one over each magnetic polarity (just above the spines of the nulls in an MCT model). Two field lines starting nearby on both sides of one stripe rapidly diverge in the volume to connect, on the other stripe, regions which are very far apart. The way field lines diverge in the central part of the QSLs, where the strongest mapping distortions are present, suggests to call this region a **hyperbolic flux tube** (HFT, Titov et al. 2002). The HFT generalizes the concept of separator. The HFT starts as an elongated stripe over one polarity; it is transformed progressively to a cross shape in the volume; then it ends in an elongated stripe over the other polarity (this stripe involved the other branch of the cross). A scheme of the cross-section is:



The QSL shape is robust. For example, the same, simply thinner, shape is found for a larger value of Q in Fig. 7. Also, if we modify the distribution of the magnetic field at the boundary (or the distribution of the electric currents in the volume), the spatial location of QSLs smoothly follow these changes (Démoulin et al. 1996a; Aulanier et al. 2005). This stability of the QSLs comes from their definition: they are derived from the integration of the magnetic

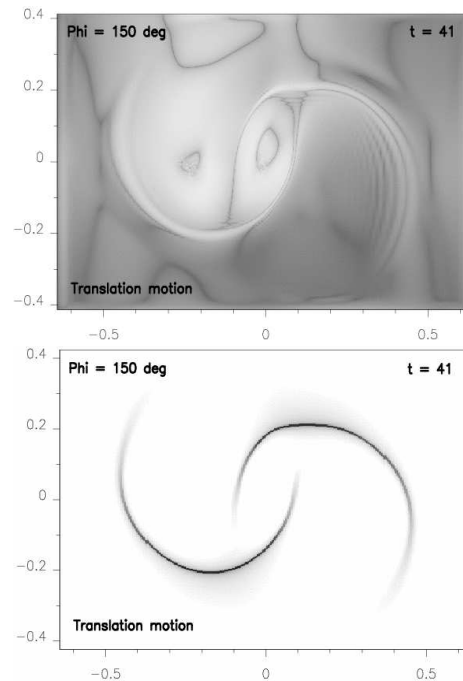


Figure 8. Formation of current layers at QSLs in a configuration comparable to Fig. 7. The left magnetic polarity of the central bipole has been displaced by a small amount ($\Delta y = 0.05$). Both panels are drawn at the “photospheric” level. **Top:** The absolute value of the current density (stronger currents are whiter). Besides distributed currents formed by the shearing motions, current layers are present at the QSLs. **Bottom:** The trace of the QSLs is shown with $\log Q$ with larger values darker (from Aulanier et al. 2005).

field (field lines) and so they are defined by the global properties of the magnetic configuration (rather than by local ones as for magnetic nulls and bald patches).

The formation of a strong current layer in any QSL is expected with almost any kind of boundary motion, as conjectured analytically by Démoulin et al. (1996a). The main reason is that the magnetic stresses of very distant regions are brought close to one another, typically over the QSL thickness. However, Titov et al. (2003) and Galsgaard et al. (2003) concluded that the formation of current layers at QSLs occurs only when special flows are present at the boundaries (creating stagnation-type flow in the volume). This result was argued by Démoulin (2005); in fact the numerical simulations of Galsgaard et al. (2003) considered very broad initial QSLs, then only weak currents did form there and they get rapidly negligible compare to the currents formed by the boundary motions. So, Galsgaard et al. (2003) did not studied the currents associated to the QSLs initially present in the field since these currents are very weak due to very broad QSLs. In fact, they studied the build up of currents associated to other much thinner QSLs which are formed dynamically by the boundary motions. These results extend those of Longcope & Strauss (1994) and Milano et al.

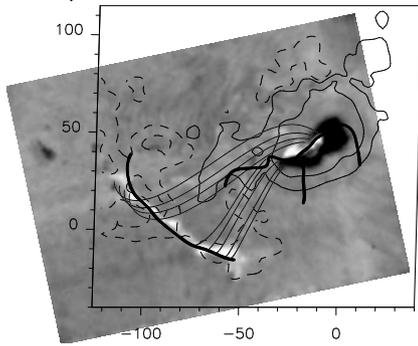


Figure 9. Example of comparison between $H\alpha$ flare ribbons (white) and the chromospheric trace of computed QSLs (thick black lines). Isocontours of the magnetogram are shown with continuous/dashed lines for positive/negative values. Some computed coronal field lines located at the borders of the QSLs are added. The connectivity organization is comparable to Figs. 6 & 7 (from Bagalá et al. 1995).

(1999); these authors found the formation of thin current layers, in an initially uniform field, by imposing at the boundary vortex flows with a stagnation point in between.

When thin QSLs are present in the initial configurations, the numerical simulations of Aulanier et al. (2005) do show that narrow current layers generically develop at the QSLs, whatever the footpoint motions are and even for relatively small displacements (Fig. 8). Of course, the precise current distribution in the QSLs depends on the type of motions imposed, but the strongest currents develop generically where the QSLs are the thinnest, namely at the HFT. The current layer at the HFT gets thinner and stronger with time; then, significant reconnection occurs only when the currents reach the dissipative scale. This implies that electric currents around QSLs may be gradually amplified in time only if the QSLs are broader than the dissipative scale; in particular, this excludes magnetic energy storage on long time scale related with current sheet formation on separatrices.

5.3. Observational tests

When magnetic energy is released in the corona, a significant part of this energy is transported along field lines by thermal conduction fronts and/or energetic particles toward the lower atmosphere. Such energy is detected as $H\alpha$ and/or UV flare brightenings. For all the flares studied so far, the brightenings are found along, or just nearby, the intersection of QSLs with the chromosphere (e.g. Fig. 9). The brightenings are also connected by magnetic field lines, just as expected by magnetic reconnection theory (Fig. 6). Moreover, the QSLs define regions much more restricted in length than the separatrices computed using the source model (Section 3), in agreement with the observed extension of brightenings which are related only to a small portion of separatrices

(Démoulin et al. 1997; Mandrini et al. 1997).

The heating of the chromosphere implies a so-called “evaporation” process which produces dense coronal plasma confined to the reconnected loops. The flare loops have been found in the close vicinity of the field lines present on the sides of QSLs. Moreover, when two sets of loops are observed, they are located as in one panel of Fig. 6 (Mandrini et al. 1996, 1997; Schmieder et al. 1997; Bagalá et al. 2000). The pre-reconnected loops are usually not dense enough to be observed, except in the case where they belong to an emerging flux (then they are observed as an arch filament system in $H\alpha$).

After testing the QSL theory in several simple configurations, where two interacting bipoles could clearly be identified, the theory has been used to understand more complex cases. For example, a complex magnetic configuration was associated with transition region brightenings (Fletcher et al. 2001a). The hot coronal loops were found to extend along the computed QSLs, while the transition region brightenings were found close to the QSL intersections with the photosphere. Furthermore, the authors found that the element abundance of the brightenings depends on the type of topological structure present. The brightenings associated with bald-patch separatrices (a subset of QSLs) had abundances closer to photospheric values, while those associated with other QSLs had abundances closer to coronal values. The difference was associated with the different atmospheric height at which magnetic reconnection occurs (i.e. chromosphere or corona).

QSLs are expected to play a key role in the very small events that contribute to coronal heating. Because most of the photospheric magnetic flux is confined to thin flux tubes, very thin QSLs are present in the corona with a thickness much smaller than the flux tube size (Démoulin & Priest 1997). However, testing precisely the role of QSLs in small scale events is limited by both the spatial resolution and the sensitivity of the instruments. Nevertheless, a correlation between the $H\alpha$ and the soft X-ray emissions of an AR with the computed QSLs was successfully found outside flaring times by Wang et al. (2000).

QSLs are also a key to understand the location of energy release in larger scale configurations, such as partial reconnection between two ARs creating interconnecting arcs. In the case studied by Bagalá et al. (2000), an interconnecting X-ray arc was associated with QSLs just as it would be for a normal flare loop. First reconnection is driven “quietly” by the rotation of one of the involved ARs; then, “dynamically” by a flare in the other AR.

Where does the magnetic energy come from? The magnetic energy available for flaring is associated with non-potential magnetic fields and so with the presence of electric currents. Indeed, concentrated electric currents have been found in the studied flares; they are located at the border of the QSLs (see Démoulin et al. 1997; Mandrini et al. 1997, and references therein). Moreover, two cur-

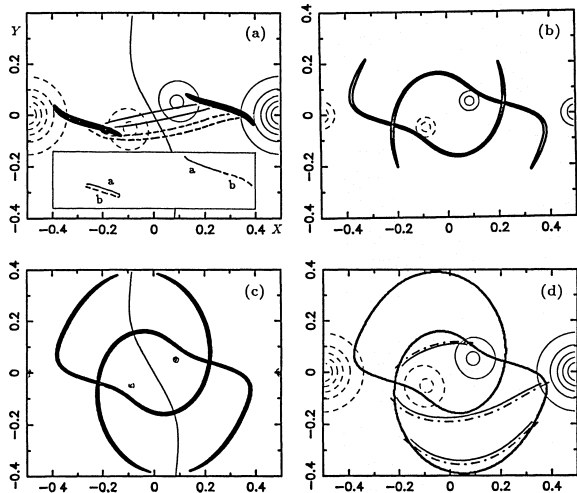


Figure 10. Comparison of the QSLs and separatrix footprint at the “photosphere” for a potential magnetic field defined by four submerged magnetic charges located in a plane. (a-c) The QSLs are represented by thick lines (isocontours N). (d) The separatrices are computed with the field line linkage to the charges. The QSLs extend more along the separatrices as the charges are less deep, from (a) to (c). Some field lines are added in panels (a,d). The selected configuration is globally bipolar (nearly straight inversion line) to emphasize the differences since the QSLs are much broader and less extended than in configurations with a more curved inversion line (from Démoulin et al. 1996b).

rent kernels of opposite sign, linked by modeled coronal field lines, are usually present. This indicates that the energy is presumably stored in the magnetic field associated with these field-aligned currents.

6. COMPARISON OF THE TOPOLOGICAL MODELS

The earlier studies of magnetic topology started with few magnetic charges, then the charges were submerged below the photosphere in order to better fit the observed magnetograms (source model, Section 3). The MCT model took another strategy by concentrating the observed flux in point-like regions with charges located at the magnetogram level (Section 4). Finally, the QSL concept was developed to compute the magnetic topology without modifying the observed magnetogram (as well as for theoretical reasons, Section 5). How are these different approaches related? Let us consider a magnetic configuration created by magnetic charges. A source model converges to the MCT model in the limit when all the charges are at the same depth: the same nulls and separatrices are defined, simply a different horizontal plane is frequently used to draw the separatrices (it is the magnetogram level for the source model, while it is the plane of charges for the MCT model). In practice, the largest difference between the two models is rather due to the dif-

ference in strength associated to each charge. There are usually more differences with a model computing QSLs, since the charges are not needed to define Q (Eq. 1), but the comparison can be done with the charge model as well. Let us bring progressively the charges to the magnetogram level. As the submerged charge depth decreases, the QSLs are present along a larger portion of the separatrices (for a constant threshold on N or Q), and at the limit of charges located at the magnetogram level, the QSLs are simply separatrices (Fig. 10). More generally, QSLs converge to separatrices in the limit where the photospheric unipolar regions are separated by flux free regions ($B_n = 0$).

In an MCT model $B_n = 0$ everywhere at the magnetogram level, except at discrete points (where B_n is infinite). This procedure usually removes the bald patches, while it creates many null points in the magnetogram plane. Most of the topology deduced from the MCT model originates in these new nulls (since the coronal nulls are much less numerous). The first advantage of the MCT is to obtain more easily the magnetic topology (mostly limited to the search of nulls in a plane, followed by the analysis of their spines and fans, then of the separators). The second advantage is that it splits always the coronal volume in a finite number of connectivity domains, from which the flux evolution of the domains, so the reconnection rate, can be analyzed. However, is an MCT model only limited to a point-charge description of any magnetogram? While used so far, it does not, since it only requires that the magnetogram be splitted in a finite number of unipolar regions and that these regions are surrounded with sufficient flux-free parts to host the prone and upright nulls. So what the MCT modeling requires is a modification of the B_n magnetogram, setting the low $|B_n|$ values to zero (the corresponding flux can be associated to the unipolar regions). This is the most delicate step of the MCT model.

Computing the QSLs of a magnetic field requires to compute a huge amount of field lines. This computation can be accelerated by using a refinement algorithm which progressively computes field lines only where the thin QSLs are located. Still it is more expensive in computation time than an MCT model. Moreover the magnetic topology is not as strictly defined, the squashing degree Q is usually continuous. However, Q is sharply peaked with very thin and elongated regions having Q many orders of magnitudes larger than in most other locations so the extension of the QSL depends only weakly on the Q threshold selected. Also, the QSLs do not split the coronal volume in connectivity domains. In an evolving configuration, the reconnected flux can only be monitored, by following the evolution of the QSLs (e.g. by following their footprints like it is done for flare ribbons). The main advantage of QSLs is that they can be computed with any magnetic extrapolation technique and with any theoretical model. If separatrices are present in the analyzed field, they are found as the highest Q values and with the thinnest width (both are limited by the numerical precision used). The QSL width is very sensitive to the magnetic flux present in the regions surrounding the

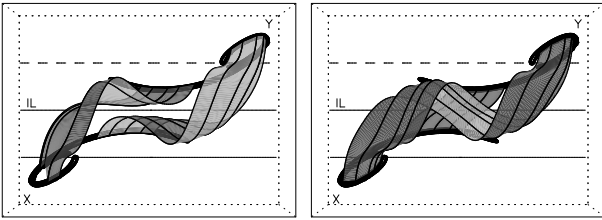


Figure 11. Perspective view of a twisted configuration with the footprints of the QSLs on the lower boundary shown with thick black lines (isocontours of N). The "magnetogram" is very simple as outline by the inversion line (IL) and the straight isocontours of the vertical field component. Still very thin QSLs are present. Each panel shows two sets of field lines computed from the borders of the QSLs (adapted from Démoulin et al. 1996b).

unipolar regions (where $B_n = 0$ is imposed in the MCT model), but also to the distributions of the unipolar regions (Démoulin & Priest 1997).

The above three different analysis of the magnetic topology applies to any magnetic field which is dominantly defined by the presence of strong flux concentrations at the boundary, a frequent case in the solar atmosphere. However, the presence of electric currents contributes also to the coronal field. If they are weak enough, they simply shift the separatrix and QSL locations, but when they are strong enough they can create new QSLs. This is most easily seen with a simple model, which has a magnetogram so uniform that only one positive and one negative unipolar region can be defined. Still QSLs are present between the twisted region and the upper (resp. lower) arcade (Fig. 11). The footprints of the QSLs have characteristic J shapes organized according to the sign of the magnetic twist. Such QSLs have no equivalent in a source or MCT model. Examples of such J-shaped ribbons have been reported in prominence eruptions. For example, the eruption, analyzed by Williams et al. (2005), has flare ribbons of two kinds (see their Fig. 2a,c): four ribbons (similar to QSL footprints in Fig. 6) and two J-shaped ribbons (similar to QSL footprints in Fig. 11).

Finally there is one important point which needs to be clarified: the location of the flare loops. All the flares analyzed with the QSLs have found the flare loops at the borders of the QSLs (Section 5.3), so within connectivity domains of the MCT model. However, Longcope & Klapper (2002) associated the three flare loops to three separators. To clarify the point, in the simplified model of Fig. 6, the QSL studies found the flare loops close to the two sets of field lines drawn in one or the other panel; while in the MCT studies, each flare loop is related to a separator (it is located just in the middle of the two sets of field-lines in one panel of Fig. 6). The approach used in analyzing the observations, MCT or QSL, is not really relevant in this debate, even if the use of a different model has probably influences on the conclusions. Rather, the physics involved and finally the test with observations are the relevant points. Even if magnetic reconnection occurs

only at the separator (or at the HFT in the QSL approach), I still believe that the soft X-ray & UV flare loops will not trace the separator. Even in the close vicinity of the separator (say ≈ 1 Mm), a field line has usually a shape more similar to other field lines of the same connectivity domain than to the separator. Also, the amount of magnetic flux is negligible in the region where field lines have the shapes of the separator (as the magnetic flux going close to a null point). During the reconnection, flux tubes in an opposite pair of domains will reconnect and will rapidly be ejected from the region of reconnection (at typically the Alfvén speed) into the other pair of domains. Moreover, these reconnected flux tubes will not be observable immediately because of too low density. It is only when the "evaporation" process succeeds to fill the reconnected flux tubes that they are observable. Then, I expect the flare loops inside the connectivity domains with foot-points far from the separator foot-points, but within a distance lower than or of the order of few Mm from the separatrices/QSLs (if the non-potentiality of the coronal field is taken into account well enough).

ACKNOWLEDGMENTS

I thank Cristina Mandrini for correcting the manuscript.

REFERENCES

- Aly, J. J. 1990, in *The Dynamic Sun*, 176
- Aulanier, G., Démoulin, P., Schmieder, B., Fang, C., & Tang, Y. H. 1998, *Solar Physics*, 183, 369
- Aulanier, G., DeLuca, E. E., Antiochos, S. K., McMullen, R. A., & Golub, L. 2000, *ApJ*, 540, 1126
- Aulanier, G., Parlat, E., & Démoulin, P. 2005, *A&A*, in press
- Bagalá, L. G., Mandrini, C. H., Rovira, M. G., & Démoulin, P. 2000, *A&A*, 363, 779
- Bagalá, L. G., Mandrini, C. H., Rovira, M. G., Démoulin, P., & Héroux, J. C. 1995, *Solar Physics*, 161, 103
- Barnes, G., Longcope, D. W., & Leka, K. D. 2005, *ApJ*, 629, 561
- Baum, P. J. & Bratenahl, A. 1980, *Solar Physics*, 67, 245
- Beveridge, C., Longcope, D. W., & Priest, E. R. 2003, *Solar Physics*, 216, 27
- Beveridge, C., Priest, E. R., & Brown, D. S. 2002, *Solar Physics*, 209, 333
- Billinghurst, M. N., Craig, I. J. D., & Sneyd, A. D. 1993, *A&A*, 279, 589
- Brown, D. S. & Priest, E. R. 1999, *Solar Physics*, 190, 25
- . 2001, *A&A*, 367, 339
- Bungey, T. N., Titov, V. S., & Priest, E. R. 1996, *A&A*, 308, 233
- Close, R. M., Parnell, C. E., Mackay, D. H., & Priest, E. R. 2003, *Solar Physics*, 212, 251

- Démoulin, P. 2005, *Advances in Space Research*, in press
- Démoulin, P., Bagalá, L. G., Mandrini, C. H., Hénoux, J. C., & Rovira, M. G. 1997, *A&A*, 325, 305
- Démoulin, P., Hénoux, J. C., & Mandrini, C. H. 1994a, *A&A*, 285, 1023
- Démoulin, P., Hénoux, J. C., Priest, E. R., & Mandrini, C. H. 1996a, *A&A*, 308, 643
- Démoulin, P., Mandrini, C. H., Rovira, M. G., Hénoux, J. C., & Machado, M. E. 1994b, *Solar Physics*, 150, 221
- Démoulin, P. & Priest, E. R. 1997, *Solar Physics*, 175, 123
- Démoulin, P., Priest, E. R., & Lonie, D. P. 1996b, *JGR*, 101, 7631
- Démoulin, P., van Driel-Gesztelyi, L., Schmieder, B., et al. 1993, *A&A*, 271, 292
- Delannée, C. & Aulanier, G. 1999, *Solar Physics*, 190, 107
- Finn, J. M. & Lau, Y. 1991, *Physics of Fluids B*, 3, 2675
- Fletcher, L., López Fuentes, M. C., Mandrini, C. H., et al. 2001a, *Solar Physics*, 203, 255
- Fletcher, L., Metcalf, T. R., Alexander, D., Brown, D. S., & Ryder, L. A. 2001b, *ApJ*, 554, 451
- Gaizauskas, V., Mandrini, C. H., Démoulin, P., Luoni, M. L., & Rovira, M. G. 1998, *A&A*, 332, 353
- Galsgaard, K., Titov, V. S., & Neukirch, T. 2003, *ApJ*, 595, 506
- Gorbachev, V. S., Kelner, S. R., Somov, B. V., & Shvarts, A. S. 1988, *Soviet Astronomy*, 32, 308
- Gorbachev, V. S. & Somov, B. V. 1988, *Solar Physics*, 117, 77
- . 1989, *Soviet Astronomy*, 33, 57
- Greene, J. M. 1988, *JGR*, 93, 8583
- Hénoux, J. C. & Somov, B. V. 1987, *A&A*, 185, 306
- Karpen, J. T., Antiochos, S. K., & Devore, C. R. 1991, *ApJ*, 382, 327
- Lau, Y. T. 1993, *Solar Physics*, 148, 301
- Lau, Y.-T. & Finn, J. M. 1990, *ApJ*, 350, 672
- Longcope, D. W. 2001, *Physics of Plasmas*, 8, 5277
- . 2005, *Living Rev. Solar Phys.*, in press, <http://www.livingreviews.org/>
- Longcope, D. W. & Klapper, I. 2002, *ApJ*, 579, 468
- Longcope, D. W., McKenzie, D., Cirtain, J., & Scott, J. 2005, *ApJ*, 630, 596
- Longcope, D. W. & Silva, A. V. R. 1998, *Solar Physics*, 179, 349
- Longcope, D. W. & Strauss, H. R. 1994, *ApJ*, 437, 851
- Low, B. C. 1987, *ApJ*, 323, 358
- . 1992, *A&A*, 253, 311
- Low, B. C. & Wolfson, R. 1988, *ApJ*, 324, 574
- Mandrini, C. H., Démoulin, P., Bagalá, L. G., et al. 1997, *Solar Physics*, 174, 229
- Mandrini, C. H., Démoulin, P., Hénoux, J. C., & Machado, M. E. 1991, *A&A*, 250, 541
- Mandrini, C. H., Démoulin, P., Rovira, M. G., de La Beaujardiere, J.-F., & Hénoux, J. C. 1995, *A&A*, 303, 927
- Mandrini, C. H., Démoulin, P., Schmieder, B., Deng, Y. Y., & Rudawy, P. 2002, *A&A*, 391, 317
- Mandrini, C. H., Démoulin, P., van Driel-Gesztelyi, L., et al. 1996, *Solar Physics*, 168, 115
- Mandrini, C. H., Rovira, M. G., Démoulin, P., et al. 1993, *A&A*, 272, 609
- Milano, L. J., Dmitruk, P., Mandrini, C. H., Gómez, D. O., & Démoulin, P. 1999, *ApJ*, 521, 889
- Molodenskii, M. M. & Syrovatskii, S. I. 1977, *Soviet Astronomy*, 21, 734
- Pariat, E., Aulanier, G., Schmieder, B., et al. 2004, *ApJ*, 614, 1099
- Pontin, D. I., Priest, E. R., & Longcope, D. W. 2003, *Solar Physics*, 212, 319
- Priest, E. R., Bungey, T. N., & Titov, V. S. 1997, *Geophys. Astrophys. Fluid Dynamics*, 84, 127
- Priest, E. R. & Démoulin, P. 1995, *JGR*, 100, 23443
- Schindler, K., Hesse, M., & Birn, J. 1988, *JGR*, 93, 5547
- Schmieder, B., Aulanier, G., Démoulin, P., et al. 1997, *A&A*, 325, 1213
- Schrijver, C. J., Hagenaar, H. J., & Title, A. M. 1997, *ApJ*, 475, 328
- Schrijver, C. J. & Title, A. M. 2002, *Solar Physics*, 207, 223
- Somov, B. 1992, *Physical processes in Solar Flares* (Kluwer Academic Publishers, Dordrecht, Holland)
- Sweet, P. A. 1958, in *IAU Symp. 6: Electromagnetic Phenomena in Cosmical Physics*, 123
- Titov, V. S. 2005, in *Reconnection of Magnetic Fields* (eds. J. Birn and E.R. Priest) (Cambridge University Press, Cambridge, UK)
- Titov, V. S. & Démoulin, P. 1999, *A&A*, 351, 707
- Titov, V. S., Galsgaard, K., & Neukirch, T. 2003, *ApJ*, 582, 1172
- Titov, V. S., Hornig, G., & Démoulin, P. 2002, *JGR*, 107, SSH 3, 1
- Titov, V. S., Priest, E. R., & Démoulin, P. 1993, *A&A*, 276, 564
- van Driel-Gesztelyi, L., Hofmann, A., Démoulin, P., Schmieder, B., & Csepura, G. 1994, *Solar Physics*, 149, 309
- Vekstein, G. E. & Priest, E. R. 1992, *ApJ*, 384, 333
- Wang, H., Yan, Y., Sakurai, T., & Zhang, M. 2000, *Solar Physics*, 197, 263
- Williams, D. R., Török, T., Démoulin, P., van Driel-Gesztelyi, L., & Kliem, B. 2005, *ApJ*, 628, L163
- Wolfson, R. 1989, *ApJ*, 344, 471
- Zwingmann, W., Schindler, K., & Birn, J. 1985, *Solar Physics*, 99, 133